Aalborg Universitet

Voltage Regulation Enhancement of DC-MG Based on Power Accumulator Battery Test System

MPC-Controlled Virtual Inertia Approach

Long, Bo; Zeng, Wei; Rodriguez, Jose; Guerrero, Josep M.; Chong, Kil To

Published in:
IEEE Transactions on Smart Grid

DOI (link to publication from Publisher):
10.1109/TSG.2021.3113306

Publication date:
2022

Document Version
Accepted author manuscript, peer reviewed version

Link to publication from Aalborg University

Citation for published version (APA):
Long, B., Zeng, W., Rodriguez, J., Guerrero, J. M., & Chong, K. T. (2022). Voltage Regulation Enhancement of DC-MG Based on Power Accumulator Battery Test System: MPC-Controlled Virtual Inertia Approach. *IEEE Transactions on Smart Grid*, *13*(1), 71-81. https://doi.org/10.1109/TSG.2021.3113306

General rights
Copyright and moral rights for the publications made accessible in the public portal are retained by the authors and/or other copyright owners and it is a condition of accessing publications that users recognise and abide by the legal requirements associated with these rights.

- Users may download and print one copy of any publication from the public portal for the purpose of private study or research.
- You may not further distribute the material or use it for any profit-making activity or commercial gain
- You may freely distribute the URL identifying the publication in the public portal -

Take down policy
If you believe that this document breaches copyright please contact us at vbn@aub.aau.dk providing details, and we will remove access to the work immediately and investigate your claim.

This article has been accepted for publication in a future issue of this journal, but has not been fully edited. Content may change prior to final publication. Citation information: DOI 10.1109/TSG.2021.3113306, IEEE Transactions on Smart Grid

Voltage Regulation Enhancement of DC-MG Based on Power Accumulator Battery Test System: MPC-Controlled Virtual Inertia Approach

Bo Long, *Member, IEEE*, Wei Zeng, *Student Member, IEEE*, José Rodríguez, *Life Fellow, IEEE*

Josep M. Guerrero *Fellow, IEEE,* Kil To Chong, *Member, IEEE*

***Abstract*—In a DC-microgrid (DC-MG) composed of a power accumulator battery test system (PABTS), owing to the low inertia of DC capacitance, the charging and discharging of a PABTS can easily cause DC-link voltage fluctuations, which may jeopardize the system stability. Hence, a virtual inertia control (VIC) strategy is proposed to suppress these fluctuations and enhance the stability of the DC-MG. The VIC method is realized in a bidirectional grid-connected converter (BGCC), which combines VIC and model predictive control (MPC). The proposed method can provide inertia support during the transient state and enhance the dynamic characteristics of the DC-link voltage. A prediction model is established that uses the variation range of the DC-link voltage as the constraint, and the output of VIC as well as voltage deviations as optimization objectives. The desired DC-link current increment is calculated using the prediction model to change the input DC current reference of the VIC. To validate the effectiveness of the proposed method, hardware-in-the-loop (HIL) experiments are performed, and the results indicate that MPC-VIC is superior to the existing VIC methods in terms of inertia support and the DC-link voltage variation suppression of PABTS DC-MGs.**

***Index Terms*— Bidirectional grid-connected converter, DC-MG, model predictive control, virtual inertia control.**

I. Introduction

OWING to the rapid development of electric vehicles (EVs), the performance and service life of batteries in EVs directly affect their large-scale industrialization. For the upcoming years, battery performance may be the single

Manuscript received May 31, 2021; revised August 19, 2021; accepted September 14, 2021. This paper is sponsored by the Fundamental Research Funds for the Central Universities of China (NO. ZYGX2019J033), Key R & D plan of science and technology department of Sichuan province (20ZDYF2816), State Key Laboratory of Control and Simulation of Power System Generation Equipment, China (SKLD20M11), Guangdong Basic and Applied Basic Research Foundation, (2021A1515010666), Tsinghua University, China, and by the VELUX FOUNDATIONS under the VILLUM Investigator Grant Center for Research on Microgrids (CROM) (Award Ref. No.: 25920): (Corresponding Author: Bo Long, Kil To Chong.)

Bo Long and Wei Zeng, are with the School of Mechanical and Electrical Engineering, University of Electronic Science and Technology of China (UESTC) 611731, China, and with the Yangtze Delta Region Institute (Huzhou), UESTC, Huzhou, 313001, P. R. China, and also with institute of electronic and information engineering of UESTC in Guangdong, 523808 (e-mail: longbouestc1980@126.com; 201952040608@std.uestc.edu.cn).

Kil To Chong is with the Department of Electronics and Information Engineering, Jeonbuk National University, Jeonju 54896, South Korea, (e-mail: kitchong@jbnu.ac.kr).

J. Rodriguez is with the Faculty of Engineering, Universidad Andres Bello, Santiago 8370146, Chile (e-mail: jose.rodriguez@unab.cl).

Josep M. Guerrero is with the Department of Energy Technology, Aalborg University, Aalborg DK-9220, Denmark. (email: joz@et.aau.dk).

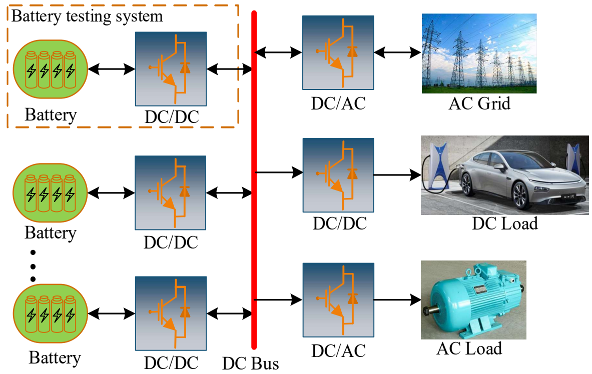

Fig. 1. Configuration of PABTS-based DC-MG.

biggest risk for EV manufacturers and purchasers. Evaluating the performance of EV batteries has become a key issue in battery technology. Batteries that fail to live up to their expected performance could cause large financial losses, and perhaps even a loss of consumer confidence that may endanger the EV industry. With so much riding on battery performance, EV and hybrid-electric vehicle (HEV) batteries must be tested as accurately and thoroughly as possible before widely deployed. A better way is to use a power accumulator battery test system (PABTS) that can simulate an actual vehicle use as accurately as possible. With the help of such a system, the power batteries can be tested in controlled environments and the whole tests can run automatically, unattended for hours or days at a time, providing vastly more test data at greatly reduced expense versus actual driving tests [1, 2]. Thus, PABTS plays a vital role in EV battery industry.

The test operation of a PABTS includes two types: energy consumption and energy saving. For the energy-consuming test, the output power is typically dissipated by resistance. For the energy-saving test, in PABTS AC-MG, the output test power of the battery is recovered to the grid via a DC-DC converter and a grid-connected converter; hence, the energy dissipated during the discharging test is not wasted.

To avoid unnecessary energy wastage, an energy recovery (ER) PABTS is presented, in which many parallel-connected PABTSs, DC loads, and bidirectional grid-connected converters (BGCCs) are utilized to form a DC-MG (as shown in Fig. 1). Therefore, the stability of the special DC-MG is jeopardized by insufficient inertia support. Fig. 1 shows the DC-MG with an ER-PABTS, where multiple PABTS are connected in parallel via a bidirectional DC/DC converter through a DC bus, and the DC-MG is connected to the grid via a BGCC. In

1949-3053 (c) 2021 IEEE. Personal use is permitted, but republication/redistribution requires IEEE permission. See http://www.ieee.org/publications_standards/publications/rights/index.html for more information.
Authorized licensed use limited to: Aalborg Universitetsbibliotek. Downloaded on September 24,2021 at 08:42:38 UTC from IEEE Xplore. Restrictions apply.

This article has been accepted for publication in a future issue of this journal, but has not been fully edited. Content may change prior to final publication. Citation information: DOI 10.1109/TSG.2021.3113306, IEEE Transactions on Smart Grid

contrast to the existing ER-PABTS AC-microgrid (AC-MG), where each parallel-connected PABTS is equipped with a DC-DC converter and a DC-AC converter that forms an AC MG, the PABTS with a DC-DC converter comprises only one energy conversion stage, which simplifies the power circuit topology and improves the energy recovery efficiency. As the rated power of each PABTS is different, when performing charge or discharge current test control, power fluctuations will occur in the traditional DC-MG, which may aggravate the fluctuation of the DC-link voltage, thereby jeopardizing the system stability [3-5]. Therefore, ensuring the stability of the DC-link voltage of the PABTS DC-MG while performing charge and discharge current tests of the power batteries is particularly important.

Studies regarding the stability analysis of PABTS DC-MGs are scarce; nonetheless, their solution can be obtained based on studies pertaining to DC-MGs, AC-MGs, and hybrid-MGs. The most recent study regarding the stability improvements of MGs suggest that they can be classified into three categories: non-virtual inertia control (NO-VIC)[6], increased virtual inertia control [7], and adaptive virtual inertia control (A-VIC) [8, 9]. Many studies pertaining to non-inertia control for system stabilization have been performed. In [10], deviations in the power or voltage of DC-MGs were used to stabilize the DC-link voltage. As a basic control technique for load current sharing in traditional DC-MGs, droop control is vital to DC-link voltage stabilization [11-13]. However, it is difficult to balance between voltage deviation and current sharing accuracy.

In addition to current sharing, owing to droop control, the DC-link voltage deviation may increase with the load changes. Hence, several solutions have been proposed to mitigate this issue [14-16]. In [14], the current sharing accuracy and DC-link voltage restoration were improved through an improved droop control of low-bandwidth communication. In [15], a closed-loop control strategy based on droop characteristics that can achieve accurate power distributions in both islanded and grid-connected DC-MGs was proposed. In [16], an observer-based DC voltage drop and current feedforward control strategy was proposed to effectively improve the dynamic response of DC-link voltage control by observers.

Inertia control is a typical method for increasing system stability. It stabilizes the voltage and frequency of the AC-MG and smooths the DC-link voltage variations in the DC-MG. In general, well-known methods for increasing inertia can be classified into two categories. One is to install an energy storage system (ESS) for the system [17], and the other is to utilize a virtual synchronous generator (VSG) to mimic the inertia characteristics of a synchronous generator (SG) with the BGCC [18].

Energy storage devices include batteries and supercapacitors. In [19, 20], J. Fang, Y *et al.* included a supercapacitor to provide transient compensation when the load was connected abruptly, and the supercapacitor improved the transient response of the DC-MG. However, the direct integration of supercapacitors requires a higher rated voltage, which is expensive. In [18], to suppress frequency and voltage fluctuations and enhance the AC-MG stability, a novel MPC-controlled VSG for an ESS was introduced, which can provide inertia support during transient states and enhance the dynamic characteristics of system voltage and frequency. However, it has not been applied to DC-MG and it needs an additional ESS. In [21], a state-of-charge (SOC) was embedded with a frequency-power droop control loop in a multi-agent manner to regulate active power in an AC-MG. In [22], N. Zhi *et al.* proposed a virtual DC machine control strategy for a DC-MG based on the SOC to dynamically balance power and SOC.

Currently, virtual inertia control, as a mature control method, has been widely used in AC-MGs and hybrid MGs [23-25]. In fact, a wind turbine has been implemented in the DC-MG system to increase the system inertia. In [7, 26], X. Zhu *et al* realized virtual inertia control in a wind turbine by switching the slope value of the maximum power point tracking curves. The other acts on the converter via virtual inertia control. Based on the virtual inertia control (VIC) of a VSG in AC-MGs [9, 27-29], VIC in DC-MGs is proposed. However, it only operates in the grid-connected mode, and for islanded DC-MGs, inertia support is lost. In addition, Yang *et al.* [30] investigated the oscillation tendency of the DC-MG voltage, improved the damping characteristics, and stabilized the DC voltage through negative feedback and VIC.

In general, adaptive inertia control optimizes the system stability by changing the system parameters. In [31], a self-tuning algorithm was used to continuously search for the optimal parameters during a virtual synchronous machine operation to minimize the amplitude and rate of frequency change as well as the power flowing through the ESS. However, the nonlinear characteristics of adaptive inertia control may easily affect the system stability. In [32], a combined control with an adaptive change in the inertia coefficient and damping coefficient was proposed to optimize the system dynamics. However, the parameter adaptability can be further improved by specifying piecewise functions. Therefore, many scholars have proposed intelligent schemes. In [17] and [33], the virtual inertia coefficient was adjusted using fuzzy logic; however, the optimal selection of the fuzzy rules remained challenging. In [34] and [35], intelligent algorithms such as bang-bang and neural predictive control were proposed and used to adaptively adjust the inertia and damping parameters. Nevertheless, the abovementioned adaptive inertia control has not been applied to the DC-MG. We may focus on this issue in our future studies.

Based on the recently published results regarding DC-MG modeling [36] and its stability, conventional VIC method could provide virtual inertia support of the DC-MG by mimicking the behavior of a virtual DC machine (VDCM). However, it could not minimize the DC-link voltage variations. To compensate this research gap, considering that MPC controller has the merits of multi-step prediction as well as multi-objective optimization capabilities, which is more suitable for inertia support control and multi-objective optimization within output constraints. Thereby, combining MPC with VIC could offer optimal solution for PABTS DC-MG. In this paper, a new MPC-VIC is proposed herein to enhance the system stability. First, a prediction model is established by setting the DC-link voltage changing rate as a constraint, and the voltage deviation and VIC output as the optimization objectives. Subsequently,

1949-3053 (c) 2021 IEEE. Personal use is permitted, but republication/redistribution requires IEEE permission. See http://www.ieee.org/publications_standards/publications/rights/index.html for more information.
Authorized licensed use limited to: Aalborg Universitetsbibliotek. Downloaded on September 24,2021 at 08:42:38 UTC from IEEE Xplore. Restrictions apply.

This article has been accepted for publication in a future issue of this journal, but has not been fully edited. Content may change prior to final publication. Citation information: DOI 10.1109/TSG.2021.3113306, IEEE Transactions on Smart Grid

the prediction model is used to calculate the optimal current increment required at the next sampling time to change the input current reference of the VIC to enhance the system anti-interference capability. In conclusion, the main contributions of this research are summarized as follows:

1) Conventional two-stage energy conversion PABTS AC-MG has the drawbacks of high overall system cost and low energy recovery efficiency. To solve this problem, a PABTS DC-MG operating only in grid-connected mode, which features with single-stage energy conversion, low cost, less volume and high efficiency, is proposed.
2) To enhance the inertia support of the PABTS DC-MG, a MPC-VIC strategy for a BGCC is proposed, including inertia and damping control. Different with traditional DC-MG [9], where its reference virtual current is constant and its anti-interference capability of the system is limited. The proposed MPC-VIC provides inertia support for the transient response of the DC-MG and suppresses fluctuations in the DC-link voltage. Thus, the system stability is enhanced. This significantly benefits the frequent charging and discharging current test control of the batteries in a DC-MG.
3) Different with our previous work in [15], the virtual inertia support in PABTS-DC MG is realized by the AC-grid and a BGCC controlled by MPC-VIC method, which does not need an additional ESS and greatly saves the system cost.

The remainder of this paper is organized as follows: Section II describes the configurations of the PABTS DC-MG and the concept of inertia regulation. To achieve an optimal control of the VSG in a DC-MG, a MPC-VIC prediction model is established. The cost function and its solutions are presented in Section III. Sections IV and V present the simulation and experimental verification results, respectively. Finally, the concluding remarks are presented in Section VI.

II. PABTS DC-MG and Inertia Control

A. System Specifications

As shown in Fig. 2, the DC-MG of the test system is composed of power battery packs, DC/DC converters, DC-link capacitors C_{dc}, a BGCC, L-filters, and related power electronic devices. The main circuit of the BGCC uses a three-phase full-bridge converter, where L is the input filter inductance, r is the equivalent series resistance of L, i_0 is the DC output current, i_{dc} is the DC link current of the BGCC, u_{dc} is the DC-link voltage of the DC-MG, v_{abc} is the utility grid voltage, and i_{abc} is the grid current.

As shown in Fig. 2, each battery pack is an independent test unit, and they may operate in the discharge or charging mode. To simplify the analysis, constant current discharge or charging test control is considered, which is realized by a bidirectional DC/DC converter connected to the DC bus. The inconsistency of the battery charging and discharging tests leads to DC-link voltage fluctuations. Therefore, a BGCC is used to maintain the power balance of the DC-MG and ensure the stability of the DC-link voltage via a bidirectional energy exchange with the AC grid.

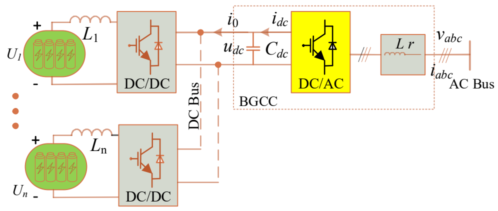

Fig. 2. Simplified circuit of PABTS DC-MG.

B. Inertia Control of DC-MG

In an AC-MG, the frequency and voltage fluctuations at the PCC are caused by power fluctuations at the power generation site and user loads. Excessive frequency fluctuations may cause system instability. To enhance the anti-interference capability of the system and increase the system inertia, a VSG control converter is typically used to simulate the primary frequency modulation, inertia, and damping characteristics similar to those of a synchronous generator. The typical equation for the VSG control strategy is as follows:

$$P_{ref} = P_0 + k(\omega_0 - \omega_g) \quad (1)$$

$$J\omega_0 \frac{d\omega_m}{dt} = P_{ref} - P_e - D\omega_0(\omega_m - \omega_0) \quad (2)$$

The active-power-frequency droop (*P-f*) equation is shown in (1), where P_{ref} is the mechanical power reference of the VSG, P_0 is the rated value of the active power, k is the active droop coefficient, ω_0 is the rated output frequency, and ω_g is the grid angular frequency. Equation (2) represents the motion equation of the mechanical rotor, where J is the rotational inertia, ω_m is the reference angular frequency, P_e is the electromagnetic power, and D is the damping coefficient that represents the damping characteristics of the VSG.

Similarly, in a DC-MG, to prevent power fluctuations caused by battery charging and discharging, VSG control can be introduced, in which the AC grid can provide inertia support to the DC-MG. Compared with the AC-MG, the DC-link voltage is the only parameter in the DC-MG that reflects the system power balance, which requires inertia support to suppress voltage fluctuations.

To obtain good dynamic characteristics and start-up characteristics of the PABTS DC-MG, the primary frequency regulation characteristics of the SG were simulated. The droop control method is widely used in the DC-MG and has been investigated extensively for power sharing and DC-link voltage regulation. The $I-U$ droop control can be expressed as

$$i_{dc}^{ref} = k_d(u_0 - u_{dc}) \quad (3)$$

where u_0 is the rated DC-link voltage, u_{dc} is the DC-link voltage, k_d is the droop coefficient, and i_{dc}^{ref} is the reference virtual current. Because the inertia of the bus capacitor is limited, it is insufficient to rely solely on the DC-link capacitor to suppress power fluctuations. Therefore, the virtual capacitor C_{vir} must be increased.

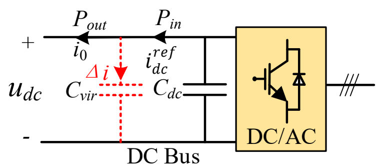

Fig. 3. Diagram of DC-MG with virtual inertia.

1949-3053 (c) 2021 IEEE. Personal use is permitted, but republication/redistribution requires IEEE permission. See http://www.ieee.org/publications_standards/publications/rights/index.html for more information.
Authorized licensed use limited to: Aalborg Universitetsbibliotek. Downloaded on September 24,2021 at 08:42:38 UTC from IEEE Xplore. Restrictions apply.

This article has been accepted for publication in a future issue of this journal, but has not been fully edited. Content may change prior to final publication. Citation information: DOI 10.1109/TSG.2021.3113306, IEEE Transactions on Smart Grid

As shown in Fig. 3, the additional fluctuation power ΔP is absorbed by the virtual capacitor. In this case, the absorbed virtual power is expressed as

$$\Delta P = C_{vir} u_{vir}^{*} \frac{du_{vir}^{*}}{dt} = P_{in} - P_{out} \quad (4)$$

where u_{vir}^{*} is the reference voltage of the virtual capacitor. Therefore, the current of the virtual capacitor Δi in Fig. 3 can be calculated as follows:

$$\Delta i = C_{vir} \frac{du_{vir}^{*}}{dt} = i_{dc}^{ref} - i_0 \quad (5)$$

where i_0 is the DC-link current. To prevent voltage oscillation, a damping current that is opposite to the direction of voltage variation is introduced. Therefore, (5) can be rewritten as

$$C_{vir} \frac{du_{vir}^{*}}{dt} = i_{dc}^{ref} - i_0 - i_D \quad (6)$$

where i_D is the damping current, which is proportional to the difference between the voltage of C_{vir} and the rated voltage. The damping current should be greater when the voltage fluctuation is increased such that it can effectively inhibit voltage fluctuations. By substituting (3) into (6), (6) can be updated as follows:

$$C_{vir} \frac{du_{vir}^{*}}{dt} = k_d(u_0 - u_{dc}) - i_0 - k_D(u_{vir}^{*} - u_0) \quad (7)$$

As shown in (7), when the DC-link power fluctuates owing to the charging and discharging current tests of the batteries, because of the virtual inertia coefficient C_{vir}, the bidirectional AC/DC converter prevents the change in the DC-link voltage by absorbing and releasing active power. The damping coefficient k_D further suppresses the frequency oscillation, and the DC-link voltage can be adjusted based on the droop coefficient k_D.

III. Design of MPC-VIC Controller

The traditional DC-MG virtual inertia control method includes a virtual inertia link, voltage, and current dual-loop control. However, when the DC-link voltage fluctuates significantly, the voltage regulation capability of the conventional VIC [32] is limited. Therefore, we propose a joint adjustment of the VIC and MPC (Naming, MPC-VIC). The proposed MPC-VIC could realize multi-step prediction, which has less tracking error for the DC-link voltage, and the DC-link voltage can restore to the steady-state with faster time response under disturbances. Moreover, MPC-VIC can handle several control objectives in the cost function, which provides a direct solution.

Fig. 4 shows a block diagram of the proposed MPC-VIC, which comprises VIC control, MPC control, and voltage-current dual-loop control. The principle of MPC control is described as follows: The dual-loop control includes voltage outer-loop control and current inner-loop control. u_d and u_q are the d-axis and q-axis components of v_{abc}, respectively. i_d and i_q are the d-axis and q-axis components of i_{abc}, respectively. i_d^{*} and i_q^{*} are the current references of i_d and i_q, respectively. MPC-VIC detects changes in the DC-link voltage. Based on the system's prediction model, it can predict the compensation current Δi_{dc} that the DC-MG requires during voltage fluctuations. Consequently, the DC-link voltage balance capability with a bidirectional AC-DC converter is enhanced.

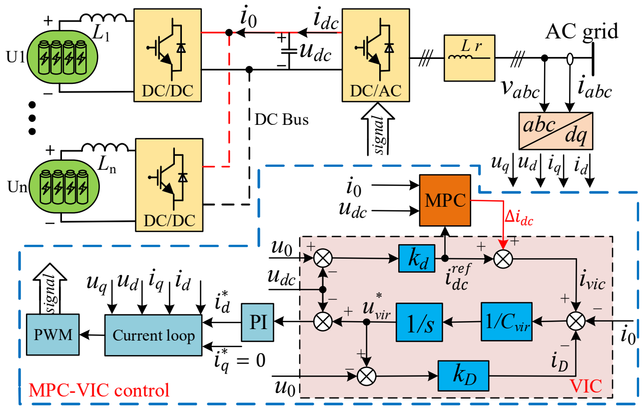

Fig. 4. Block diagram of proposed MPC-VIC method.

A. Prediction Model of VIC

To effectively realize the DC-link voltage stability of the DC-MG, a mathematical model of the MPC-VIC is established. First, we rewrite (7) as follows:

$$\frac{du_{vir}^{*}}{dt} = \frac{1}{C_{vir}} i_{dc}^{ref} - \frac{1}{C_{vir}} i_0 - \frac{k_D}{C_{vir}} (u_{vir}^{*} - u_0) \quad (8)$$

Subsequently, we rewrite (8) into a state-space model as follows:

$$\begin{cases} \dot{u}(t) = \frac{1}{C_{vir}} i_{dc}^{ref}(t) - \frac{k_D}{C_{vir}} u(t) - \frac{1}{C_{vir}} i_0(t) \\ y(t) = u(t) \end{cases} \quad (9)$$

where $u(t) = u_{vir}^{*} - u_0$. Based on (9), fluctuations in the DC-link input current will cause power imbalance and fluctuations in the DC-link voltage. In (9), $u(t)$ is regarded as the state variable, the virtual current reference $i_{dc}^{ref}(t)$ is used as the input, and the DC-link current $i_0(t)$ is regarded as the system disturbance.

To eliminate the introduction of the integral term to reduce or eliminate the static error, (9) is converted into a discrete incremental model using the Duhamel method [37] as follows:

$$\begin{cases} \Delta u(k+1) = A\Delta u(k) + B_u \Delta i_{dc}^{ref}(k) + B_d \Delta i_0(k) \\ y(k+1) = y(k) + \Delta u(k+1) \end{cases} \quad (10)$$

In the equation above,

$$A = e^{-\frac{k_D}{C_{vir}} T_s},\ B_u = \frac{1}{C_{vir}} \int_0^{T_s} e^{-\frac{k_D}{C_{vir}} \tau} d\tau,\ B_d = \frac{1}{C_{vir}} \int_0^{T_s} e^{-\frac{k_D}{C_{vir}} \tau} d\tau$$

where $\Delta u(k+1)$ is the control output, which indicates the variation in the DC-link voltage; T_s is the sampling time. Hence, the DC-link voltage variations $\Delta u(k)$, virtual current reference changes $\Delta i_{dc}^{ref}(k)$, and DC-link current changes can be written as

$$\begin{cases} \Delta u(k) = u(k) - u(k-1) \\ \Delta i_{dc}^{ref}(k) = i_{dc}^{ref}(k) - i_{dc}^{ref}(k-1) \\ \Delta i_0(k) = i_0(k) - i_0(k-1) \end{cases} \quad (11)$$

1949-3053 (c) 2021 IEEE. Personal use is permitted, but republication/redistribution requires IEEE permission. See http://www.ieee.org/publications_standards/publications/rights/index.html for more information.
Authorized licensed use limited to: Aalborg Universitetsbibliotek. Downloaded on September 24,2021 at 08:42:38 UTC from IEEE Xplore. Restrictions apply.

This article has been accepted for publication in a future issue of this journal, but has not been fully edited. Content may change prior to final publication. Citation information: DOI 10.1109/TSG.2021.3113306, IEEE Transactions on Smart Grid

Considering the control precision and calculation burden in implementation, a three-step prediction was applied [38-40]. Therefore, the voltage prediction equation can be expressed as

$$\boldsymbol{Y}_3(k+1|k) = \boldsymbol{S_A}\Delta u(k) + \boldsymbol{I}y(k) + \boldsymbol{S_u}\Delta\boldsymbol{i}_{dc}^{ref}(k) + \boldsymbol{S_d}\Delta\boldsymbol{i_0}(k) \quad (12)$$

where $\boldsymbol{Y_3}(k+1|k)$ is the output of the three-step prediction of the system at instant k, and $\Delta\boldsymbol{i}_{dc}^{ref}(k)$ is the increment sequence of the control variable. $\boldsymbol{Y_3}$ and $\Delta\boldsymbol{i}_{dc}^{ref}(k)$ are defined as follows:

$$\boldsymbol{Y_3}(k+1|k) \overset{\text{def}}{=} \begin{bmatrix} y(k+1|k) \\ y(k+2|k) \\ y(k+3|k) \end{bmatrix}, \Delta\boldsymbol{i}_{dc}^{ref}(k) \overset{\text{def}}{=} \begin{bmatrix} \Delta i_{dc}^{ref}(k) \\ \Delta i_{dc}^{ref}(k+1) \\ \Delta i_{dc}^{ref}(k+2) \end{bmatrix} \quad (13)$$

Where

$$\boldsymbol{S_A} = [A \quad \Sigma_{i=1}^{2}A^i \quad \Sigma_{i=1}^{3}A^i]^T \ , \boldsymbol{I} = [1 \quad 1 \quad 1]^T$$
$$\boldsymbol{S_d} = [B_d \quad \Sigma_{i=1}^{2}A^{i-1}B_d \quad \Sigma_{i=1}^{3}A^{i-1}B_d]^T$$
$$\boldsymbol{S_u} = \begin{bmatrix} B_u & 0 & 0 \\ \Sigma_{i=1}^{2}A^{i-1}B_u & B_u & 0 \\ \Sigma_{i=1}^{3}A^{i-1}B_u & \Sigma_{i=1}^{2}A^{i-1}B_u & B_u \end{bmatrix}$$

B. Cost Function Design

The control target for the DC-MG is to maintain a stable DC-link voltage under disturbance. When the discharge power of the batteries increases, the energy should be recovered to the grid to suppress power fluctuations. Similarly, when the charging power of the batteries increases, the energy should be absorbed from the AC grid to smooth the DC-link voltage changes and provide inertia support to the DC-MG. When the DC-link voltage fluctuates, the MPC-VIC can output the optimal compensation current to suppress DC-link voltage fluctuations based on a three-step prediction (considering the calculation expense, the three-step prediction of MPC-VIC is selected). Therefore, considering the changes in the DC-link voltage and VIC output, the cost function g is designed as follows:

$$g = \Sigma_{i=1}^{3}\left[(\lambda_1\Delta u(k+i|k))^2 + (\lambda_2\Delta i_{dc}^{ref}(k+i|k))^2\right] \quad (14)$$

where λ_1 and λ_2 represent the voltage and current change weight coefficients. $\Delta u(k+i|k)$ and $i_{dc}^{ref}(k+i|k))$ represent the voltage and current errors at time instant k. In (14), the first term ensures a fast recovery of the DC-link voltage, and the latter term is used to minimize the output cost of the VIC. The changes in the DC-link voltage should be limited to a certain range. This can be expressed as a constrained MPC problem as follows:

$$\begin{cases} \min\limits_{\Delta i_{dc}^{ref}(k)} g(\Delta u(k), \Delta i_{dc}^{ref}(k)) \\ s.t.\ \Delta u(k+i+1|k) = A\Delta u(k+i|k) + B_u\Delta i_{dc}^{ref}(k+i) \\ \qquad +B_d\Delta i_0(k+i) \\ \qquad \Delta u(k|k) = \Delta u(k) \\ u(k+i+1|k) = u(k+i|k) + \Delta u(k+i|k),\ i \geq 1 \\ y_{min}(k+i) \leq y(k+i|k) \leq y_{max}(k+i) \quad \forall k > 0 \end{cases} \quad (15)$$

Therefore, the cost function in (14) can be rewritten as

$$g\left(\Delta u(k), \Delta i_{dc}^{ref}(k)\right) = \left\|\boldsymbol{\Gamma_y}(\boldsymbol{Y_3}(k+1|k) - \boldsymbol{R}(k+1))\right\|^2 + \left\|\boldsymbol{\Gamma_i}\Delta\boldsymbol{i}_{dc}^{ref}(k)\right\|^2 \quad (16)$$

where $\boldsymbol{\Gamma_y}$ and $\boldsymbol{\Gamma_i}$ represent the weight coefficient matrices of the voltage and current change, respectively; $\boldsymbol{R}(k+1)$ is the desired output reference at $k+1$. Here, it denotes the DC-link voltage variations (0 as expected). The coefficient matrices $\boldsymbol{\Gamma_y}$, $\boldsymbol{\Gamma_i}$, and the reference matrix $\boldsymbol{R}$ are expressed as follows:

$$\begin{cases} \boldsymbol{\Gamma_y} = diag\{\lambda_1, \lambda_1, \lambda_1\} \\ \boldsymbol{\Gamma_i} = diag\{\lambda_2, \lambda_2, \lambda_2\} \\ \boldsymbol{R}(k+1) = [0\ 0\ 0]^T \end{cases} \quad (17)$$

C. Control Strategy Solution

Equation (15) can be transformed into a quadratic programming (QP) problem. The cost function should be transformed into a quadratic standard form of $z^T\boldsymbol{H}z - g^Tz$, and the control quantity constraint should be rewritten as a linear standard from of $\boldsymbol{C}z \geq \boldsymbol{b}$, where $z = \Delta\boldsymbol{i}_{dc}^{ref}(k)$ is an independent variable of the optimization problem. The intermediate variable $\boldsymbol{E}$ is defined as follows:

$$\boldsymbol{E}(k+1|k) \overset{\text{def}}{=} \boldsymbol{R}(k+1) - \boldsymbol{S_A}\Delta\boldsymbol{u}(k) - \boldsymbol{I}y(k) - \boldsymbol{S_d}\Delta\boldsymbol{i_0}(k) \quad (18)$$

After substituting (18) into (12), the cost function in (16) can be rewritten as

$$\begin{aligned} g &= \left\|\boldsymbol{\Gamma_y}(\boldsymbol{S_u}\Delta\boldsymbol{i}_{dc}^{ref}(k) - \boldsymbol{E}(k+1|k))\right\|^2 + \left\|\boldsymbol{\Gamma_i}\Delta\boldsymbol{i}_{dc}^{ref}(k)\right\|^2 \\ &= \Delta\boldsymbol{i}_{dc}^{ref}(k)^T\boldsymbol{S_u}^T\boldsymbol{\Gamma_y}^T\boldsymbol{\Gamma_y}\boldsymbol{S_u}\Delta\boldsymbol{i}_{dc}^{ref}(k) \\ &\quad +\Delta\boldsymbol{i}_{dc}^{ref}(k)^T\boldsymbol{\Gamma_i}^T\boldsymbol{\Gamma_i}\Delta\boldsymbol{i}_{dc}^{ref}(k) \\ &\quad -2\boldsymbol{E}(k+1|k)^T\boldsymbol{\Gamma_y}^T\boldsymbol{\Gamma_y}\boldsymbol{S_u}\Delta\boldsymbol{i}_{dc}^{ref}(k) \\ &\quad +\boldsymbol{E}(k+1|k)^T\boldsymbol{\Gamma_y}^T\boldsymbol{\Gamma_y}\boldsymbol{E}(k+1|k) \end{aligned} \quad (19)$$

$\boldsymbol{E}(k+1|k)^T\boldsymbol{\Gamma_y}^T\boldsymbol{\Gamma_y}\boldsymbol{E}(k+1|k)$ is independent of variable $\Delta\boldsymbol{i}_{dc}^{ref}(k)$; therefore, for the optimization of the QP problem, (19) is equivalent to

$$g = \Delta\boldsymbol{i}_{dc}^{ref}(k)^T\boldsymbol{L}\Delta\boldsymbol{i}_{dc}^{ref}(k) - \boldsymbol{M}(k+1|k)^T\Delta\boldsymbol{i}_{dc}^{ref}(k) \quad (20)$$

where

$$\boldsymbol{H} = \boldsymbol{S_u}^T\boldsymbol{\Gamma_y}^T\boldsymbol{T_y}\boldsymbol{S_u} + \boldsymbol{\Gamma_i}^T\boldsymbol{\Gamma_i}$$
$$\boldsymbol{M}(k+1|k) = 2\boldsymbol{S_u}^T\boldsymbol{\Gamma_y}^T\boldsymbol{\Gamma_y}\boldsymbol{E}(k+1|k) \quad (21)$$

Subsequently, the DC-link voltage constraint in (15) is transformed into a linear standard in the form of $\boldsymbol{C}z \geq \boldsymbol{b}$.

$$\boldsymbol{Y_{min}}(k+1) \leq \boldsymbol{Y}(k+1|k) \leq \boldsymbol{Y_{max}}(k+1) \quad (22)$$

where

$$\boldsymbol{Y_{min}}(k+1) = [y_{min}(k+1) \quad y_{min}(k+2) \quad y_{min}(k+3)]^T$$
$$\boldsymbol{Y_{max}}(k+1) = [y_{max}(k+1) \quad y_{max}(k+2) \quad y_{max}(k+3)]^T \quad (23)$$

Substituting (12) into (22), the DC-link voltage constraints can be rewritten as

$$\begin{bmatrix} -\boldsymbol{S_u} \\ \boldsymbol{S_u} \end{bmatrix}\Delta\boldsymbol{i}_{dc}^{ref}(k) \geq \boldsymbol{b}(k) \quad (24)$$

where

$$\boldsymbol{b}(k) = \begin{bmatrix} \boldsymbol{S_A}\Delta\boldsymbol{u}(k) + \boldsymbol{I}y(k) + \boldsymbol{S_d}\Delta\boldsymbol{i_0}(k) - \boldsymbol{Y_{max}}(k+1) \\ -(\boldsymbol{S_A}\Delta\boldsymbol{u}(k) + \boldsymbol{I}y(k) + \boldsymbol{S_d}\Delta\boldsymbol{i_0}(k)) + \boldsymbol{Y_{min}}(k+1) \end{bmatrix} \quad (25)$$

1949-3053 (c) 2021 IEEE. Personal use is permitted, but republication/redistribution requires IEEE permission. See http://www.ieee.org/publications_standards/publications/rights/index.html for more information.
Authorized licensed use limited to: Aalborg Universitetsbibliotek. Downloaded on September 24,2021 at 08:42:38 UTC from IEEE Xplore. Restrictions apply.

This article has been accepted for publication in a future issue of this journal, but has not been fully edited. Content may change prior to final publication. Citation information: DOI 10.1109/TSG.2021.3113306, IEEE Transactions on Smart Grid

Based on (20)-(25), the MPC optimization problem (15) with the constraint of the approximate voltage change is transformed into the QP problem expressed as follows:

$$\min_{\Delta \boldsymbol{i}_{dc}^{ref}(k)} \ \Delta \boldsymbol{i}_{dc}^{ref}(k)^T \boldsymbol{H} \Delta \boldsymbol{i}_{dc}^{ref}(k) - \boldsymbol{M}(k+1|k)^T \Delta \boldsymbol{i}_{dc}^{ref}(k) \quad (26)$$

$$\text{Satisfy } \boldsymbol{C_u} \Delta \boldsymbol{i}_{dc}^{ref}(k) \geq \boldsymbol{b}(k)$$

where

$$\boldsymbol{C_u} = [-\boldsymbol{S_u} \quad \boldsymbol{S_u}]^T \quad (27)$$

Based on (21), it is clear that $\boldsymbol{H} \geq 0$. Therefore, the QP problem (26) has one solution ($\Delta \boldsymbol{i}_{dc}^{opt}(k)$) for any weighting matrix $\boldsymbol{\Gamma_y} \geq 0$ and $\boldsymbol{\Gamma_i} \geq 0$.

D. Stability Analysis

In the proposed method, the reference input power of the VIC is affected by the result of the MPC algorithm (see Fig. 4), and the stability of the MPC algorithm directly affects the control performance. To verify whether the DC-link voltage can be restored under the charging and discharging current test control of the batteries, the stability of the MPC algorithm must be analyzed. This is realized by setting its result as the power setting value of the VIC into the state equation.

For MPC with input constraints, to analyze the system stability, a case-by-case discussion should be considered.

(1). If the solution of (26) is within the boundary of the feasible region, then the original model becomes an unconstrained model, and the optimal control rate is

$$\Delta \boldsymbol{i}_{dc}^{ref}(k)^* = \boldsymbol{K}(\boldsymbol{R}(k+1) - \boldsymbol{S_A}\Delta \boldsymbol{u}(k) - \boldsymbol{I}y(k) - \boldsymbol{S_d}\Delta \boldsymbol{i_0}(k))$$
$$= \boldsymbol{K}\big(\boldsymbol{R}(k+1) - (\boldsymbol{S_A}+\boldsymbol{I})\Delta \boldsymbol{u}(k) - \boldsymbol{S_d}\Delta \boldsymbol{i_0}(k) - \boldsymbol{I}\boldsymbol{u}(k-1)\big) \quad (28)$$

where

$$\boldsymbol{K} = \boldsymbol{H}^{-1}\boldsymbol{S_u}^T\boldsymbol{\Gamma_y}^T\boldsymbol{\Gamma_y} \quad (29)$$

Substituting (28) into (10) yields

$$\Delta \boldsymbol{u}(k+1) = \big(A - B_u\boldsymbol{K}(\boldsymbol{S_A}+\boldsymbol{I})\big)\Delta \boldsymbol{u}(k) + B_u\boldsymbol{K}\boldsymbol{R}(k+1)$$
$$+(B_d - B_u\boldsymbol{K}\boldsymbol{S_d})\Delta \boldsymbol{i_0}(k) - B_u\boldsymbol{K}\boldsymbol{I}\boldsymbol{u}(k-1) \quad (30)$$

Let $\bar{A} = A - B_u\boldsymbol{K}(\boldsymbol{S_A}+\boldsymbol{I})$. When the absolute value of $\bar{A}$ is less than 1, the eigenvalue of $\bar{A}$ is in the unit circle, and the unconstrained MPC system is nominally asymptotically stable; otherwise, the system is stable. Moreover, the voltage deviation converges to 0. In other words, the DC-link voltage returns to its rated value.

(2). If the solution of (26) reaches the constraint boundary, i.e., when (24) has an equal sign, the input power reference value of VIC obtained by the MPC algorithm will be the upper limit of the VIC output within the allowable range. In this case, the VIC will output an active power based on this upper limit value, and the change in the DC-link voltage is primarily determined by the regulation of other units and energy storage devices in the system. In summary, to improve the voltage response dynamics, the proposed MPC-VIC algorithm can promptly adjust its output power to reduce the voltage change rate and voltage deviation when the DC-MG is disturbed. Based on the analysis above, Fig.5 shows the implementation flowchart of MPC-VIC controller illustrated in Fig. 3.

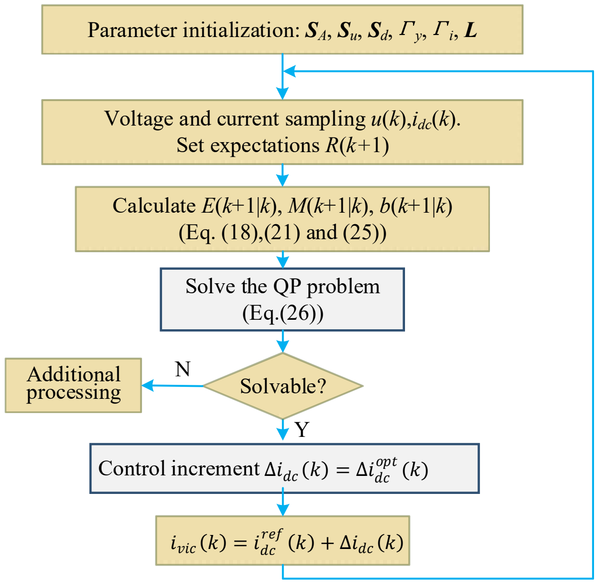

Fig. 5. Implementation flowchart of proposed MPC-VIC.

IV. Experimental Results

A. Hardware Setup

Experimental verification was performed to validate the theoretical analysis described in Section III. Owing to the parallel operation complexities of multiple power converters and power batteries, hardware-in-the-loop (HIL) testing, which mimics the behavior of the PABTS, was used because it can provide the most complex model-based design to interact with the actual environment.

In the experiment, RT-LAB (OP4050 from RT-LAB Company, Canada) was used as a real-time simulator for power-stage simulation. Similarly, MicroLabBox (dSPACE, Germany), which is a compact, multifunctional and effective development system for laboratory testing, was used for NO-VIC, A-VIC and MPC-VIC control implementation. Here, NO-VIC represents that the BGCC is controlled without virtual inertia support, where voltage-current double loop control is used [6, 41]. A-VIC stands for adaptive virtual inertia control, which adaptive changes the inertia of BGCC according to the rate of change of DC-link voltage [17, 28], and finally, MPC-VIC is the proposed method.

Fig. 6 shows the experimental setup. Models of the loads, switching devices, drive circuits, power battery packs, and power converters have been established in RT-LAB. MicroLabBox will sample RT-LAB output signals (e.g., grid current, voltage, DC-link voltage and current, and battery charge and discharge currents). The control signal is generated based on the proposed method and then input to RT-LAB. The sampling time was 40 µs. To simplify the battery test system, we set all battery discharge and charging modes to a constant current during the experiment. Consequently, a closed-loop HIL simulation platform for the MG was established.

1949-3053 (c) 2021 IEEE. Personal use is permitted, but republication/redistribution requires IEEE permission. See http://www.ieee.org/publications_standards/publications/rights/index.html for more information.
Authorized licensed use limited to: Aalborg Universitetsbibliotek. Downloaded on September 24,2021 at 08:42:38 UTC from IEEE Xplore. Restrictions apply.

This article has been accepted for publication in a future issue of this journal, but has not been fully edited. Content may change prior to final publication. Citation information: DOI 10.1109/TSG.2021.3113306, IEEE Transactions on Smart Grid

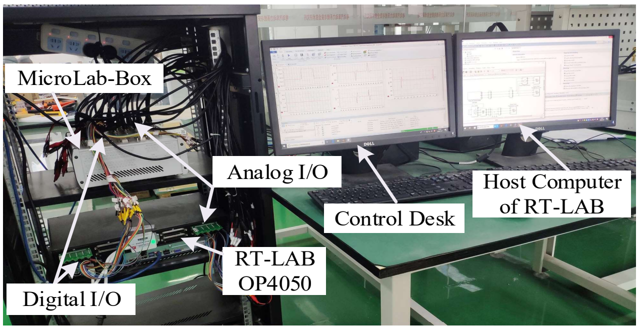

Fig. 6. Configuration of the HIL experimental platform.

The HIL test served two primary purposes: 1) to verify the validity and effectiveness of MPC-VIC for PABTS DC-MGs in utility, and 2) to evaluate the advantage of MPC-VIC over other existing methods (A-VIC [28, 42] and NO-VIC) in DC-link voltage suppression under different scenarios.

Tables I and II show the parameter specifications of the battery and the MPC-VIC controller, respectively. For the battery parameters, we refer to the power batter information of an electric vehicle company (Model-S 85 from Tesla company) as an example.

TABLE I
Parameter Specifications of Power Battery

Parameters	Value
Nominal voltage	355.2 V
Rated capacity (Ah)	145.7 Ah
Initial state-of-charge	50%

Table II
Parameter Specifications in MPC-VIC

Parameters	Symbol	Value
DC-link voltage	U_{dc}	700 VDC
Grid voltage	V_g	220 VAC
Fundamental frequency	f_o	50 Hz
Inductance	L	10 mH
DC bus capacitance	C_{dc}	1350 μF
Virtual capacitance	C_{vir}	0.5 mF
Droop coefficient	k_d	38
Damping coefficient	k_D	30
Prediction horizon	N	3
Weight factor	λ_1, λ_2	1
Sampling time	T_s	5 μ s

B. Result and Analysis

Assume that the initial state of the DC-MG is as follows: a discharge test current of 50 A is performed for battery-I, and the discharged energy is recovered to the AC grid via the BGCC (this is defined as the initial state). Therefore, the following four tests were performed to verify the effectiveness of the different control methods on the DC-voltage stabilities of the PABTS-DC-MGs. The experimental results are shown in Figs. 7-11.

Case 1: Charging Current Test Disturbance. In the initial state, to evaluate the DC-link voltage variations, a step-up charging test current of approximately 10 A was applied at 0.16 s for battery-II. The waveforms of battery-II's SOC, current, and voltage are shown in Fig. 7 (a), where its SOC increased from 50% of its initial value, and its voltage remained at approximately 355.2 V.

Fig. 7 (b) shows the dynamic response of the DC-link voltage with different control strategies. The results indicate that without inertia control, the instantaneous maximal DC-link voltage drop may reach 14 V, and that an additional overshoot occurred during the recovery process. With A-VIC, the DC-link voltage drop is reduced (approximately 10.5 V) because of the inertia support. MPC-VIC releases more inertia power than A-VIC, and the voltage variation is further reduced (approximately 8.5 V). When the DC-MG enters a steady state, MPC-VIC releases less power than A-VIC, which has a faster time response for the steady-state arrival of the system. Consequently, the suppression of the DC-link voltage fluctuation with MPC-VIC is reduced by 39.3% and 19.0% compared with those of NO-VIC and A-VIC, respectively. This verifies that the suppression performance of the DC-link voltage fluctuation with MPC-VIC is better than that with A-VIC and NO-VIC.

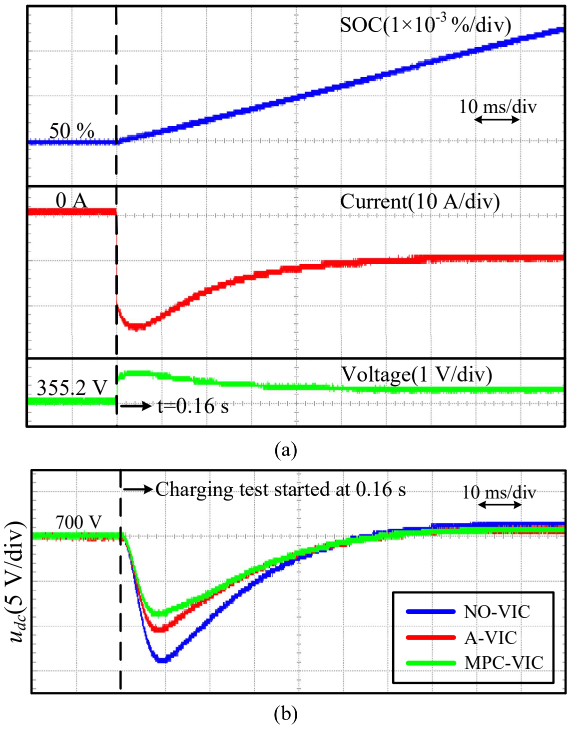

Fig. 7. DC-link voltage under charging current test of battery-II. (a) SOC, current, and battery voltage; (b) Dynamic response of the DC-link voltage with different control methods.

Case 2: Discharge Current Test Disturbance. Fig. 8 shows the experimental results under the battery-III discharge test in the initial state. A discharge current test with 10 A was implemented at 0.16 s. Fig. 8 (a) shows the SOC changes of battery-III. The SOC decreased gradually from 50% of the initial value, the discharging current was 10 A, and the battery voltage remained at approximately 355.2 V.

1949-3053 (c) 2021 IEEE. Personal use is permitted, but republication/redistribution requires IEEE permission. See http://www.ieee.org/publications_standards/publications/rights/index.html for more information.
Authorized licensed use limited to: Aalborg Universitetsbibliotek. Downloaded on September 24,2021 at 08:42:38 UTC from IEEE Xplore. Restrictions apply.

This article has been accepted for publication in a future issue of this journal, but has not been fully edited. Content may change prior to final publication. Citation information: DOI 10.1109/TSG.2021.3113306, IEEE Transactions on Smart Grid

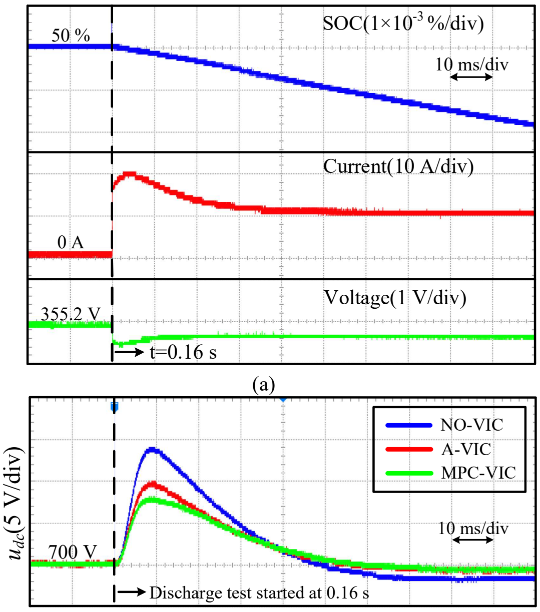

(b)

Fig. 8. DC-link voltage under discharging current test of battery-III. (a) Discharge current test of battery-III; (b) DC-link voltage with different control methods.

Fig. 8 (b) shows the transient response of the DC-link voltage with different controllers under discharge disturbance. When the discharge test was performed at 0.16 s, the input power of the system increased. Without inertia control, the DC-link voltage will increase rapidly to approximately 714 V, and voltage fluctuations will occur. By including A-VIC control, the voltage fluctuation can be reduced by 28.5%. The DC-link voltage with MPC-VIC further suppressed the voltage fluctuation by 42.5% and 19.6% compared with NO-VIC and with A-VIC. The HIL experiment further proves the effectiveness of the proposed scheme.

Case 3: DC-link Voltage Under Grid Voltage Changes. In practice, the AC grid is not always ideal. When the grid voltage fluctuates, the stability of the DC-link voltage is affected. Figs. 9 (a) and (b) show the waveform of the three-phase grid voltage when it increases by 20%. Fig. 9 (b) shows the DC-link voltage fluctuations affected by the change in the grid voltage with different control methods. When the grid voltage increased, the instantaneous DC-link voltage decreased to approximately 4.9, 3.9 and 3.2 V for the NO-VIC, A-VIC, and MPC-VIC methods. Among the abovementioned methods, the MPC-VIC method demonstrated the minimum DC-link voltage-drop.

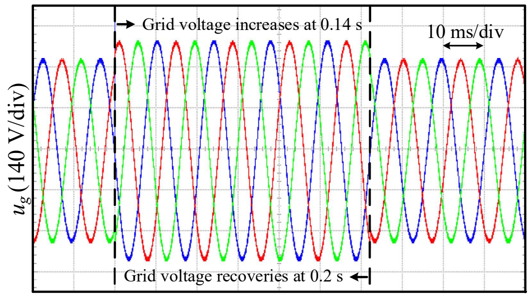

(a)

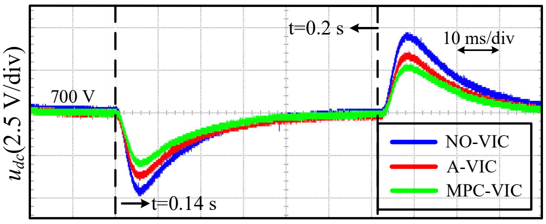

(b)

Fig. 9. DC-link voltage under grid voltage changes. (a) Three-phase grid-voltage; (b). DC-link voltage.

Case 4: DC-link Voltage Under Load Changes. To evaluate the DC-voltage stability under load changes, a 10-kW resistive load was connected at 0.14 s and removed at 0.21 s (see Fig. 10 (a)). Fig. 10 (b) shows the DC-link voltage comparison under various control schemes; as shown, the DC-link voltage decreased by approximately 20.3, 13.6, and 10.7 V for NO-VIC, A-VIC, and MPC-VIC, respectively. The proposed MPC-VIC reduced the fluctuations by 21.3% and 47.3% compared with A-VIC and NO-VIC, respectively.

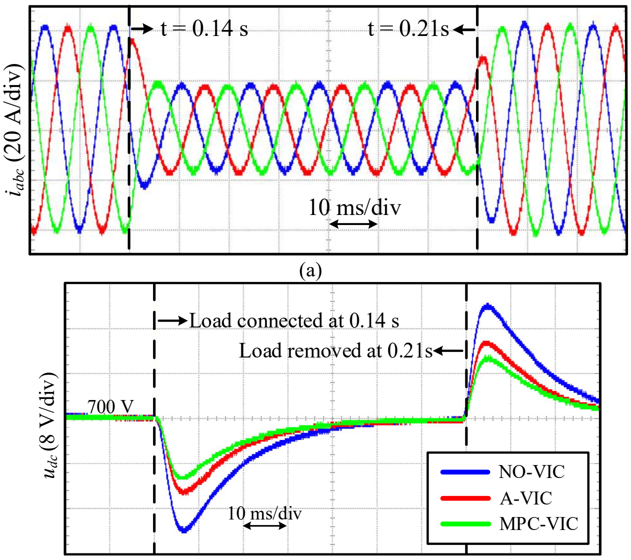

(b)

Fig. 10. DC-link voltage and grid current under load variations. (a) Three-phase grid current; (b) DC-link voltage with different control methods.

In Fig. 10 (a), when a resistive load with 10-kW is connected at 0.14 and removed at 0.21 s, the amplitude of the grid current during this period is reduced, which is because of the following reasons: In initial state, the discharging test energy of battery-I is fully recovered to the grid. When the load is connected, less test energy will be recovered, resulting in a reduction of the grid current. To show the power quality of the grid current, its harmonic distribution is given in Fig.11. The THD of the grid current without and with resistive load are 1.79% and 3.48%, respectively, which meets the grid integration requirements.

From the above four experimental scenarios, it can be seen that, when the PABTS DC-MG is influenced by the disturbances (for instance, charging and discharge current test of the batteries, grid voltage variations, and load changes), the DC-link voltage of the system with the proposed MPC-VIC can always be maintained stable, the results indicate that the

1949-3053 (c) 2021 IEEE. Personal use is permitted, but republication/redistribution requires IEEE permission. See http://www.ieee.org/publications_standards/publications/rights/index.html for more information.
Authorized licensed use limited to: Aalborg Universitetsbibliotek. Downloaded on September 24,2021 at 08:42:38 UTC from IEEE Xplore. Restrictions apply.

This article has been accepted for publication in a future issue of this journal, but has not been fully edited. Content may change prior to final publication. Citation information: DOI 10.1109/TSG.2021.3113306, IEEE Transactions on Smart Grid

proposed method has the minimum overshoot with fast time response comparing with A-VIC and NO-VIC methods.

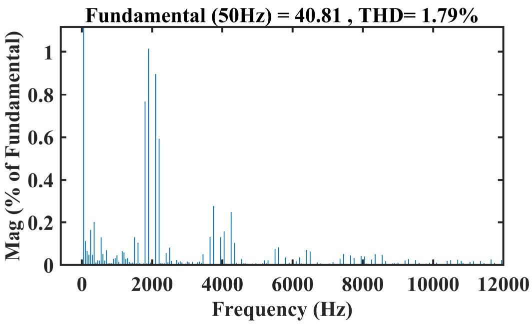

(a)

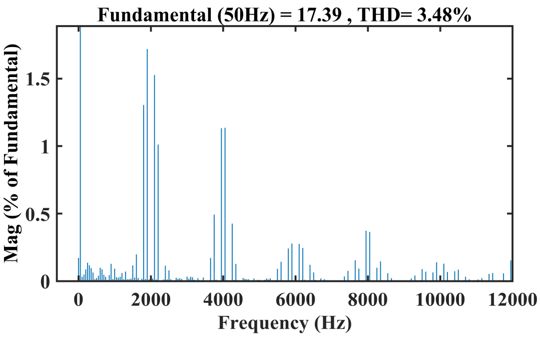

(b)

Fig. 11. THD of the grid current when a resistive load with 10-kW is connected.

V. Conclusion

To increase the inertia of a DC-MG composed of PABTS, a MPC-VIC algorithm is proposed herein to further enhance the inertia of the DC-MG. The MPC-VIC control strategy is realized by predicting the optimal current variations and superimposes it to the current reference for power fluctuation compensation. This strategy can further enhance the DC-link voltage regulation capability. Compared with the traditional inertia-supporting method, the novel MPC-VIC does not require any additional ESS. Experimental results indicated that the MPC-VIC method certified better dynamic performances in terms of DC-link voltage regulation than the NO-VIC and A-VIC methods, thereby verifying its effectiveness in inertia support and DC-link voltage stabilization. In future studies, the proposed method can be applied to other DC-MGs.

Acknowledgement

"J. Rodriguez acknowledges the support of ANID through projects FB0008, ACT192013 and 1210208".

Reference

[1] J. Nie, "Design of Power State Test System for Electric Vehicle Battery," in *2018 International Conference on Smart Grid and Electrical Automation (ICSGEA)*, 2018, pp. 16-19.

[2] L. Mihet-Popa and V. Groza, "Battery management system test platform developed for electric vehicle applications," in *The 9th IEEE International Symposium on Intelligent Signal Processing*, 2015, pp. 1-6.

[3] N. Rashidirad, M. Hamzeh, K. Sheshyekani, and E. Afjei, "A Simplified Equivalent Model for the Analysis of Low-Frequency Stability of Multi-Bus DC Microgrids," *IEEE Transactions on Smart Grid,* pp. 1-1, 2017.

[4] L. L. Fan, V. Nasirian, H. Modares, F. L. Lewis, Y. D. Song, and A. Davoudi, "Game-Theoretic Control of Active Loads in DC Microgrids," *IEEE Transactions on Energy Conversion,* vol. 31, no. 3, pp. 882-895, 2016.

[5] M. Amin and M. Molinas, "Understanding the Origin of Oscillatory Phenomena Observed between Wind Farms and HVDC Systems," *IEEE journal of emerging and selected topics in power electronics,* vol. 5, no. 1, pp. 378-392, 2017.

[6] T. Wu, C. Chang, L. Lin, G. Yu, and Y. Chang, "DC-Bus Voltage Control With a Three-Phase Bidirectional Inverter for DC Distribution Systems," *IEEE Transactions on Power Electronics,* vol. 28, no. 4, pp. 1890-1899, 2013.

[7] X. Zhu, J. Cai, Y. Wang, Y. Feng, and X. Hu, "Virtual inertia control of wind-battery-based DC micro-grid," *Proceedings of the CSEE,* 2016.

[8] D. Jiawei, Z. Jiangbin, and M. Zihan, "VSG Inertia and Damping Coefficient Adaptive Control," *2020 Asia Energy and Electrical Engineering Symposium (AEEES),* 2020.

[9] W. Wu *et al.*, "A Virtual Inertia Control Strategy for DC Microgrids Analogized with Virtual Synchronous Machines," *IEEE Transactions on Industrial Electronics,* vol. 64, no. 7, pp. 6005-6016, 2017.

[10] Vasquez *et al.*, "DC Microgrids-Part I: A Review of Control Strategies and Stabilization Techniques," *IEEE Transactions on Power Electronics,* 2016.

[11] M. Shaheed, Y. Sozer, S. Chowdhury, and J. Abreu-Garcia, "A Novel Decentralized Adaptive Droop Control Technique for DC Microgrids Based on Integrated Load Condition Processing," in *2020 IEEE Energy Conversion Congress and Exposition (ECCE)*, 2020.

[12] H. Liang, J. Ding, J. Bian, and Z. Liu, "Research on Fuzzy Droop Control of DC Microgrid Based on Consensus Algorithm," in *2020 4th International Conference on Smart Grid and Smart Cities (ICSGSC)*, 2020.

[13] L. Huang, H. Xin, Z. Wang, L. Zhang, K. Wu, and J. Hu, "Transient Stability Analysis and Control Design of Droop-Controlled Voltage Source Converters Considering Current Limitation," *IEEE Transactions on Smart Grid,* vol. 10, no. 1, pp. 578-591, 2019.

[14] Z. Yi, X. Zhao, D. Shi, J. Duan, and Z. Wang, "Accurate Power Sharing and Synthetic Inertia Control for DC Building Microgrids With Guaranteed Performance," *IEEE Access,* vol. PP, no. 99, pp. 1-1, 2019.

[15] S. Nayar and T. Ghose, "Power Sharing And Management Through Power Based Droop Control in DC microgrid," in *2019 3rd International conference on Electronics, Communication and Aerospace Technology (ICECA)*, 2019.

[16] X. Li *et al.*, "Observer-based DC Voltage Droop and Current Feed-Forward Control of a DC Microgrid," *IEEE Transactions on Smart Grid,* vol. 9, no. 5, pp. 5207-5216, Sept. 2018.

[17] T. Kerdphol, M. Watanabe, Y. Mitani, and K. Hongesombut, "Self-Adaptive Virtual Inertia Control-Based Fuzzy Logic to Improve Frequency Stability of Microgrid With High Renewable Penetration," *IEEE Access,* vol. 7, pp. 76071-76083, 2019.

[18] B. Long, Y. Liao, K. T. Chong, J. Rodríguez, and J. M. Guerrero, "MPC-Controlled Virtual Synchronous Generator to Enhance Frequency and Voltage Dynamic Performance in Islanded Microgrids," vol. 12, no. 2, pp. 953-964, 2021.

[19] J. Fang, Y. Tang, H. Li, and X. Li, "A Battery/Ultracapacitor Hybrid Energy Storage System for Implementing the Power Management of Virtual Synchronous Generators," *IEEE Transactions on Power Electronics,* pp. 1-1, 2017.

[20] R. K. Sarojini and P. Kaliannan, "Inertia Emulation Through Supercapacitor for a Weak Grid," *IEEE Access,* vol. 9, no. 99, pp. 1-1, 2021.

[21] C. Li, T. Dragicevic, J. C. Vasquez, J. M. Guerrero, and E. A. A. Coelho, "Multi-agent-based distributed state of charge balancing control for distributed energy storage units in AC microgrids," *in 2015 IEEE Applied Power Electronics Conference and Exposition (APEC),* pp. 2967-2973, 2015.

[22] N. Zhi, K. Ding, L. Du, and H. Zhang, "An SOC-based Virtual DC Machine Control for Distributed Storage Systems in DC Microgrids," *IEEE Transactions on Energy Conversion,* vol. 35, no. 3, pp. 1411-1420, Sept. 2020.

[23] Eman, Hammad, Abdallah, Farraj, Deepa, and Kundur, "On Effective Virtual Inertia of Storage-Based Distributed Control for Transient Stability," *IEEE Transactions on Smart Grid,* vol. 10, no. 1, pp. 327-336, 2019.

1949-3053 (c) 2021 IEEE. Personal use is permitted, but republication/redistribution requires IEEE permission. See http://www.ieee.org/publications_standards/publications/rights/index.html for more information.
Authorized licensed use limited to: Aalborg Universitetsbibliotek. Downloaded on September 24,2021 at 08:42:38 UTC from IEEE Xplore. Restrictions apply.

This article has been accepted for publication in a future issue of this journal, but has not been fully edited. Content may change prior to final publication. Citation information: DOI 10.1109/TSG.2021.3113306, IEEE Transactions on Smart Grid

[24] J. Liu, Y. Miura, H. Bevrani, and T. Ise, "Enhanced Virtual Synchronous Generator Control for Parallel Inverters in Microgrids," *IEEE Transactions on Smart Grid,* vol. 8, no. 5, pp. 2268-2277, Sept. 2017.

[25] T. Chen, J. Guo, B. Chaudhuri, and S. Y. Hui, "Virtual Inertia from Smart Loads," *IEEE Transactions on Smart Grid,* vol. 11, no. 5, pp. 4311-4320, 2020.

[26] X. Zhu, Z. Xie, and S. Jing, "Virtual Inertia Control and Stability Analysis of DC Micro-Grid," *Power System Technology,* 2017.

[27] D. Chen, Y. Xu, and A. Q. Huang, "Integration of DC Microgrids as Virtual Synchronous Machines Into the AC Grid," *IEEE Transactions on Industrial Electronics,* vol. 64, no. 9, pp. 7455-7466, 2017.

[28] W. Wu, Y. Chen, A. Luo, L. Zhou, and L. Yang, "A Virtual Inertia Control Strategy for Bidirectional Grid-connected Converters in DC Micro-grids," *Proceedings of the CSEE,* vol. 37, no. 2, pp. 360-371, 2017.

[29] X. Zhu, F. Meng, Z. Xie, and Y. Yue, "An Inertia and Damping Control Method of DC–DC Converter in DC Microgrids," *IEEE Transactions on Energy Conversion,* vol. 35, no. 2, pp. 799-807, 2020.

[30] Y. Yang, C. Li, J. Xu, F. Blaabjerg, and T. Dragičević, "Virtual Inertia Control Strategy for Improving Damping Performance of DC Microgrid With Negative Feedback Effect," vol. 9, no. 2, pp. 1241-1257, 2021.

[31] M. A. T. L, L. A. C. Lopes, L. A. M. T, and J. R. E. C, "Self-Tuning Virtual Synchronous Machine: A Control Strategy for Energy Storage Systems to Support Dynamic Frequency Control," *IEEE Transactions on Energy Conversion,* vol. 29, no. 4, pp. 833-840, 2014.

[32] Zhu *et al.*, "A Self-Adaptive Inertia and Damping Combination Control of VSG to Support Frequency Stability," *IEEE Transactions on Energy Conversion,* vol. 32, no. 1, pp. 397-398, 2017.

[33] Y. Kumar and R. Bhimasingu, "Fuzzy logic based adaptive virtual inertia in droop control operation of the microgrid for improved transient response," in *2017 IEEE PES Asia-Pacific Power and Energy Engineering Conference (APPEEC)*, 2017.

[34] J. Li, B. Wen, and H. Wang, "Adaptive Virtual Inertia Control Strategy of VSG for Micro-grid Based on Improved Bang-bang Control Strategy," *IEEE Access,* pp. 1-1, 2019.

[35] A. S. Mir and N. Senroy, "Self-Tuning Neural Predictive Control Scheme for Ultrabattery to Emulate a Virtual Synchronous Machine in Autonomous Power Systems," *IEEE Transactions on Neural Networks and Learning Systems,* pp. 1-12, 2019.

[36] R. Wang, Q. Sun, P. Tu, J. Xiao, Y. Gui, and P. Wang, "Reduced-Order Aggregate Model for Large-Scale Converters With Inhomogeneous Initial Conditions in DC Microgrids," *IEEE Transactions on Energy Conversion,* vol. 36, no. 3, pp. 2473-2484, 2021.

[37] J. Hubbard and B. West, "Dynamical Systems," 1993.

[38] T. Geyer and D. E. Quevedo, "Multistep Finite Control Set Model Predictive Control for Power Electronics," *IEEE Transactions on Power Electronics,* vol. 29, no. 12, pp. 6836-6846, 2014.

[39] T. Geyer and D. E. Quevedo, "Performance of Multistep Finite Control Set Model Predictive Control for Power Electronics," *IEEE Transactions on Power Electronics,* vol. 30, no. 3, pp. 1633-1644, 2015.

[40] T. Geyer and D. E. Quevedo, "Multistep direct model predictive control for power electronics — Part 2: Analysis," in *2013 IEEE Energy Conversion Congress and Exposition*, 2013, pp. 1162-1169.

[41] M. Shi, X. Chen, J. Zhou, Y. Chen, J. Wen, and H. He, "Distributed Optimal Control of Energy Storages in a DC Microgrid With Communication Delay," *IEEE Transactions on Smart Grid,* vol. 11, no. 3, pp. 2033-2042, 2020.

[42] Y. Zhang, Q. Sun, J. Zhou, L. Li, P. Wang, and J. M. Guerrero, "Coordinated Control of Networked AC/DC Microgrids With Adaptive Virtual Inertia and Governor-Gain for Stability Enhancement," *IEEE Transactions on Energy Conversion,* vol. 36, no. 1, pp. 95-110, 2021.

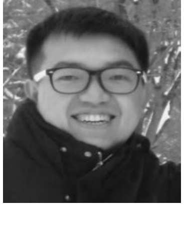

BO Long (S'08–M'10) received the B.S. degree in electrical engineering from the Xi'an Petroleum University, Xian, China, in 2001, and the Ph.D. degree in electrical engineering from Xian Jiaotong University, Shanxi, China, in 2008. He joined the Department of Power Electronics, School of Mechatronics Engineering, UESTC, in 2008, and has been promoted to an Associate Professor since 2014. From 2017 to 2018, he was a Visiting Scholar (Guest Post-Doctoral Researcher) in the area of renewable energy and microgrids with the Department of Electrical Engineering, Tsinghua University, Beijing, China. His research interests include ac/dc microgrids, grid-connected converters for renewable energy systems and DGs, model predictive control, power quality, multilevel converters, ac motor control, and resonance suppression technique for smart grid applications. He has authored over 20 SCIE-indexed journal papers and one book chapter in the area of power electronics, motor control, battery management system, and smart grid. He has seven issued and 10 pending patents. He is currently the supervisor for eleven master students, two of which have been nominated as provincial outstanding graduate student of UESTC. He is an active Reviewer for the IEEE TRANSACTIONS ON POWER ELECTRONICS, ISA TRANSACTIONS, APPLIED ENERGY, ENERGY, the IEEE TRANSACTIONS ON SMART GRID, the IEEE TRANSACTIONS ON I NDUSTRIAL ELECTRONICS, the IEEE TRANSACTIONS ON SUSTAINABLE ENERGY, and the IEEE TRANSACTIONS ON ENERGY CONVERSION.

Wei Zeng received the B.S. degree in mechanical engineering from Chongqing Technology and Business University, Chongqing, China, in 2019. He is currently pursuing the M.S. degree in mechanical engineering from University of Electronic Science and Technology of China, Chengdu, China. His current research interest is the optimization of direct microgrids, involving virtual inertia control, model predictive control, fractional order systems, and so on.

José Rodríguez (M'81-SM'94-F'10) received the Engineer degree in electrical engineering from the Universidad Tecnica Federico Santa Maria, in Valparaiso, Chile, in 1977 and the Dr.-Ing. degree in electrical engineering from the University of Erlangen, Erlangen, Germany, in 1985. He has been with the Department of Electronics Engineering, Universidad Tecnica Federico Santa Maria, since 1977, where he was a full professor and President. Since 2015 he is the President of Universidad Andres Bello in Santiago, Chile. He has co-authored two books, several book chapters, and more than 400 journal and conference papers. His main research interests include multilevel inverters, new converter topologies, control of power converters, and adjustable-speed drives. He has received a number of best paper awards from journals of the IEEE. Dr. Rodriguez is a member of the Chilean Academy of Engineering. In 2014 he received the National Award of Applied Sciences and Technology from the government of Chile. In 2015, he received the Eugene Mittelmann Award from the Industrial Electronics Society of the IEEE.

Josep M. Guerrero (S'01-M'04-SM'08-FM'15) received the B.S. degree in telecommunications engineering, the M.S. degree in electronics engineering, and the Ph.D. degree in power electronics from the Technical University of Catalonia, Barcelona, in 1997, 2000 and 2003, respectively. Since 2011, he has been a Full Professor with the Department of Energy Technology, Aalborg University, Denmark, where he is responsible for the Microgrid Research Program. From 2014 he is chair Professor in Shandong University; from 2015 he is a distinguished guest Professor in Hunan University; and from 2016 he is a visiting professor fellow at Aston University, UK, and a guest Professor at the Nanjing University of Posts and Telecommunications. From 2019, he became a Villum Investigator by The Villum Fonden, which supports the Center for Research on Microgrids (CROM) at Aalborg University, being Prof. Guerrero the founder and Director of the same center (www.crom.et.aau.dk). His research interests are oriented to different microgrid aspects, including power electronics, distributed energy-storage systems, hierarchical and cooperative control, energy management systems, smart metering and the internet of things for AC/DC microgrid clusters and islanded microgrids. Specially focused on microgrid technologies applied to offshore wind, maritime microgrids for electrical ships, vessels, ferries and seaports, and space microgrids applied to nanosatellites and spacecrafts. Prof. Guerrero is an Associate Editor for a number of IEEE TRANSACTIONS. He has published more than 600 journal papers in the fields of microgrids and renewable energy systems, which are cited more than 50,000 times. He received the best paper award of the IEEE Transactions on Energy Conversion for the period 2014-

1949-3053 (c) 2021 IEEE. Personal use is permitted, but republication/redistribution requires IEEE permission. See http://www.ieee.org/publications_standards/publications/rights/index.html for more information.
Authorized licensed use limited to: Aalborg Universitetsbibliotek. Downloaded on September 24,2021 at 08:42:38 UTC from IEEE Xplore. Restrictions apply.

This article has been accepted for publication in a future issue of this journal, but has not been fully edited. Content may change prior to final publication. Citation information: DOI 10.1109/TSG.2021.3113306, IEEE Transactions on Smart Grid

2015, and the best paper prize of IEEE-PES in 2015. As well, he received the best paper award of the Journal of Power Electronics in 2016. During six consecutive years, from 2014 to 2019, he was awarded by Clarivate Analytics (former Thomson Reuters) as Highly Cited Researcher with 50 highly cited papers. In 2015 he was elevated as IEEE Fellow for his contributions on "distributed power systems and microgrids."

Kil To Chong received the Ph.D. degree in mechanical engineering from Texas A&M University, in 1995. He is currently a Professor and the Department Head of the School of Electronics and Information Engineering and a member and the Head of the Advanced Electronics and Information Research Center, Chonbuk National University, Jeonju, South Korea. His research interests include motor fault detection and control, network system control, sensor network systems, time-delay systems, and neural networks.

1949-3053 (c) 2021 IEEE. Personal use is permitted, but republication/redistribution requires IEEE permission. See http://www.ieee.org/publications_standards/publications/rights/index.html for more information.
Authorized licensed use limited to: Aalborg Universitetsbibliotek. Downloaded on September 24,2021 at 08:42:38 UTC from IEEE Xplore. Restrictions apply.